Indicators and trends of polar cold airmass

Environmental Research Letters

LETTER

Indicators and trends of polar cold airmass

Yuki Kanno[1,2,3], John E Walsh[4], Muhammad R Abdillah[6], Junpei Yamaguchi[5] and Toshiki Iwasaki[5]

[1] Institute for Space-Earth Environmental Research, Nagoya University, Nagoya, Japan
[2] Geophysical Institute, University of Bergen, Bergen, Norway
[3] Bjerknes Centre for Climate Research, Bergen, Norway
[4] Alaska Center for Climate Assessment and Policy, University of Alaska Fairbanks, Fairbanks, Alaska, United States of America
[5] Department of Geophysics, Graduate School of Science, Tohoku University, Sendai, Japan
[6] Atmospheric Science Research Group, Faculty of Earth Science and Technology, Institut Teknologi Bandung, Bandung, Indonesia

E-mail: kanno@isee.nagoya-u.ac.jp

Keywords: climate, Arctic, indicators, cold airmass

OPEN ACCESS

RECEIVED
29 June 2018

REVISED
16 November 2018

ACCEPTED FOR PUBLICATION
27 November 2018

PUBLISHED
11 February 2019

Abstract

Trends and variations in the amount of cold airmass in the Arctic and the Northern Hemisphere are evaluated for the 60 year period, 1959–2018. The two indicators are (1) polar cold air mass (PCAM), which is the amount of air below a potential temperature threshold, and (2) negative heat content (NHC), which includes a weighting by coldness. Because the metrics of coldness are based on multiple layers in the atmosphere, they provide a more comprehensive framework for assessment of warming than is provided by surface air temperatures alone. The negative trends of PCAM and NHC are stronger (as a % per decade) when the threshold is 245 K rather than 280 K, indicating that the loss of extremely cold air is happening at a faster rate than the loss of moderately cold air. The loss of cold air has accelerated, as the most rapid loss of NHC has occurred in recent decades (1989–2018). The spatial patterns of the trends of PCAM and NHC provide another manifestation of Arctic amplification. Of the various teleconnection indices, the Atlantic Multidecadal Oscillation shows the strongest correlations with the spatially integrated metrics of moderate coldness. Several Pacific indices also correlate significantly with these indicators. However, the amount of extremely cold air mass does not correlate significantly with the indices of internal variability used here.

1. Introduction

Air temperatures in the Arctic have global significance for several reasons. First and most fundamentally, the Arctic is the heat sink for the global system that includes the atmospheric winds and ocean currents. The atmospheric waves and meridional cells, together with the system of near-surface and deep ocean currents, exhibit a spectrum of variability (including day-to-day changes of weather) as they redistribute the excess heat of the tropics to higher latitudes. Second, a characteristic of radiatively (greenhouse gas) forced climate change is that regions of low temperatures show a greater warming than regions of high temperatures. Manifestations of this differential sensitivity include polar amplification as well as a potentially stronger warming of the Arctic's coldest airmasses relative to the rate of global warming. Arctic amplification of mean temperatures is already well documented (IPCC 2013, USGCRP 2014). Third, the Arctic is the source of the airmasses that bring cold air outbreaks to middle latitudes. The most extreme cold outbreaks have impacts ranging from excessive demands for heating to mechanical failures, human well-being and even deaths. A growing body of literature has addressed the coupling between the Arctic and extreme cold outbreaks in middle latitudes (e.g. Mori *et al* 2014, Screen *et al* 2015, Overland and Wang 2018, Graham *et al* 2017, Ogawa *et al* 2018). Variations and trends of Arctic temperatures, especially at the low end of the distribution, can be expected to show an association with midlatitude cold air outbreaks in the sense that the cold outbreaks should be less severe if there is a moderation of the coldest Arctic airmasses. Finally, Arctic temperatures drive variations in the cryosphere and high-latitude ecosystems. Recent observational assessments (IPCC 2013, Overland *et al* 2017) have shown that changes in sea ice, snow cover,

permafrost and glaciers are consistent with the recent Arctic warming as measured by the mean temperatures. The recent increase of mean temperatures in the Arctic at a rate approximately double the global warming rate is consistent with global climate model simulations (IPCC 2013, Pithan and Mauritsen 2014).

Studies of Arctic temperatures, especially their trends, have tended to focus on the mean temperatures (e.g. Fyfe *et al* 2013, Overland *et al* 2017). Because (1) extreme cold has impacts on humans, wildlife, ecosystems and infrastructure, and (2) daily and extreme minimum temperatures show a stronger warming than extreme maximum temperatures (IPCC 2013, USGCRP 2014), metrics of extremely cold in the Arctic must be considered a priority for monitoring. Accordingly, this paper uses several metrics of Arctic 'coldness', including the amount of air below a threshold for extremely cold, as indicators of Arctic change. These metrics are defined in section 2. The results of an analysis of variations and trends of these indicators over the past six decades are presented in section 3. We then conclude with a discussion of linkages to other Arctic indicators and a look at the implications of the trends for the future of the Arctic and its midlatitude connections.

2. Cold airmass metrics

Most studies of Arctic air temperatures have been based solely on surface air temperature (e.g. Bekryaev *et al* 2010, AMAP 2017, Overland *et al* 2017). Reconstructions for longer periods based on proxy (paleo) indicators have also been for surface air temperature (Kaufman *et al* 2009). In the context of climate variability and change, as well as the Arctic-midlatitude connection alluded to above, the total amount of cold air in the climate system is at least as important as a metric based only on surface air temperatures. Especially when ongoing and projected climate changes are addressed in a 'global warming' framework, the total amount of atmospheric mass below (or above) a particular threshold is arguably a more meaningful indicator. While there have been evaluations of the total moisture content (precipitable water) in the Arctic (Serreze *et al* 2012), temperature indicators based on three-dimensional integrations have only recently been developed (Iwasaki *et al* 2014). The present study uses three-dimensional metrics of cold and extreme cold air in the Northern Hemisphere atmosphere. The first metric is the polar cold air mass (PCAM) amount, which is the mass of air below a prescribed threshold of potential temperature integrated over a three-dimensional domain. The second metric is the negative heat content (NHC), which is the corresponding integral with each mass element weighted by the magnitude of its potential temperature deficit relative to the prescribed threshold. In both cases, the potential temperature is used rather than the actual temperature in order to allow for the effects of adiabatic compression if the air were brought to 1000 hPa (approximately the surface). Both PCAM and the NHC have been used in previous studies (e.g. Iwasaki *et al* 2014, Kanno *et al* 2016, Kanno *et al* 2017). These previous studies include analyses of variability and trends over particular calendar months, e.g. January and geographic regions (Kanno *et al* 2016).

In formal mathematical terms, the two metrics are defined as follows. If the potential temperature threshold is denoted as θ_T, the PCAM amount at each grid point is defined as the pressure difference between the ground surface and the θ_T surface.

$$DP \equiv p_s - p(\theta_T), \tag{1}$$

where p is a pressure and p_s is a pressure at the ground surface. The PCAM amount is zero at the location where the surface potential temperature exceeds the threshold value θ_T. The unit of the PCAM amount at each grid point is hPa. The horizontal integration of PCAM amount is

$$\langle DP \rangle \equiv \frac{1}{g} \iint DPa^2 \cos\phi d\phi d\lambda, \tag{2}$$

where a is a radius of the Earth, ϕ is latitude, and λ is longitude. The spatially integrated PCAM amount is divided by the gravitational acceleration g, so that its unit is kg. The range of integration over ϕ and λ is the domain of interest, which in this case is either the Northern Hemisphere or the polar cap north of 60 °N. In subsequent sections, we refer to the 60°−90°N polar cap as 'the Arctic'. The important property of the integrated PCAM amount is its adiabatic invariant nature, i.e. it is conserved under adiabatic conditions. Its temporal changes are due only to diabatic processes such as radiative heating/cooling, latent heat release in the atmosphere, and sensible heat exchange with the underlying surface. The PCAM flux is defined similarly as the vertically integrated product of the horizontal velocity vector and DP.

The NHC, which measures the 'coldness' of the PCAM, is computed similarly, but with the vertical air column at each location broken into pressure increments dp, each of which is weighted by the deficit of potential temperature relative to θ_T:

$$\mathrm{NHC} \equiv \int_{p(\theta_T)}^{p_s} (\theta_T - \theta) dp, \tag{3}$$

followed by a horizontal integration over ϕ and λ as in (2). The units of NHC at each grid point and integrated over the spatial domain are K hPa and K kg, respectively. As is the PCAM amount, the spatially integrated NHC is an adiabatic invariant.

The evaluations of PCAM and NHC are based on the output of the 55 year Japanese Reanalysis (JRA-55), which begins in 1958 (Kobayashi *et al* 2015). The present study uses updates of JRA-55 through February 2018. JRA-55 is an atmospheric reanalysis archived at 6 h intervals on a grid with 1.25° resolution in latitude and longitude. The gridded fields are available for 37

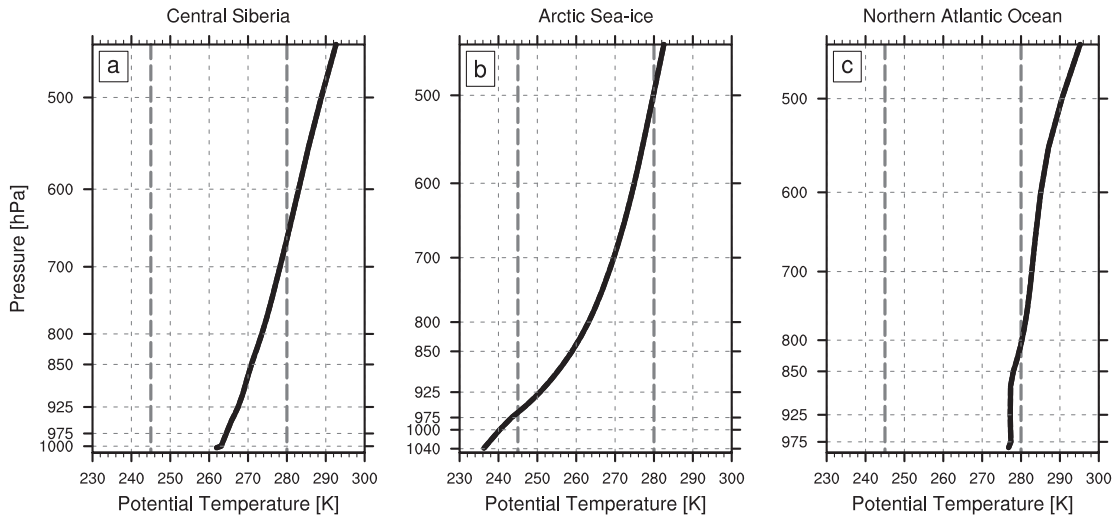

Figure 1. Vertical profiles of potential temperature on 00 UTC of 10 January, 2005. Potential temperature is spatially averaged over (a) central Siberia (80°E–90°E, 55°N–65°N), (b) Arctic sea ice (170°E–180°E, 70°N–80°N), and (c) northern Atlantic Ocean (0°E–10°E, 65°N–70°N). Gray broken vertical lines indicate potential temperature of 245 and 280 K.

pressure levels ranging from 1000 to 1 hPa. For this study, we make use of the archived fields of temperature (at all pressure levels and at 2 m above the ground—the ground surface value) and surface pressure for use in (1)–(3). The potential temperature, θ, at each pressure level is computed from the values of temperature and pressure at that level. The 6 h values of PCAM and NHC over a prescribed domain (0°−90° N or 60°–90°N) are computed for each 6 h time increment and then summed over the winter season (December–February). In the following section, we show these sums for the two domains and for two choices of the potential temperature threshold, θ_T. The seasonal sums (integrals) of PCAM and NHC are then our indicators of the amount of cold air and its coldness.

3. Results and discussion

The variations and trends of PCAM and NHC were evaluated for December–February of the 60 complete winters available from the JRA-55 reanalysis: 1958–59 through 2017–18. This section presents the results in the form of spatial maps and time series. Sensitivities to the spatial domain are addressed by showing time series and correlations for CAM and NHC over Northern Hemisphere and Arctic domains, 0°–90° and 60°–90° N, respectively. We also use two main thresholds of potential temperature, 280 and 245 K, to illustrate the sensitivity to the choice of the threshold. 280 K was adopted for use in prior studies (e.g. Iwasaki *et al* 2014, Kanno *et al* 2015, 2016) because the equatorward flow in the extratropical direct circulation at 45 °N is generally confined to the layer below 850 hPa where 280 K is a representative potential temperature (Iwasaki and Mochizuki 2012, Iwasaki *et al* 2014). The lower threshold, 245 K, can be taken as a metric for extremely cold air (−28 °C), even by Arctic standards.

In order to illustrate the potential temperature distributions that contribute to the PCAM and NHC metrics, figure 1 shows typical vertical profiles of potential temperature for the Arctic in winter, in this case for 10 January 2005. The profiles are averaged over areas of 10° longitude and 5°–10° latitude in central Siberia, the sea-ice-covered Arctic Ocean, and the ice-free North Atlantic. All three profiles contain potential temperatures below 280 K; the corresponding depths (PCAM 280 K) range from approximately 150 hPa over the North Atlantic to approximately 500 hPa over the Arctic sea ice. NHC (280 K), represented by the area between the actual profile and the vertical 280 K line in each panel, is clearly much greater over the Arctic sea ice than over the other two regions. For the cases shown in figure 1, PCAM 245 K is zero over central Siberia and the North Atlantic, where the profiles contain no values colder than 245 K. However, PCAM (245 K) is approximately 70 hPa over the Arctic sea ice. Figure 1 also illustrates different stability characteristics in the different regions. Over the Arctic sea ice, the potential temperature increases relatively rapidly in the lower troposphere, indicating that the atmosphere is statically stable. Over the ocean, on the other hand, the slow increase of potential temperature with height indicates that the atmosphere is nearly neutral, suggestive of mixing due to advection of cold air over warmer ocean.

Figure 2 shows climatological distributions of PCAM and NHC for winters of the 30 year period 1981–2010, which is the current reference period for climatological normals. Separate maps are shown for PCAM based on thresholds of (a) 280 K and (b) 245 K, for which we use the designations PCAM (280 K) and

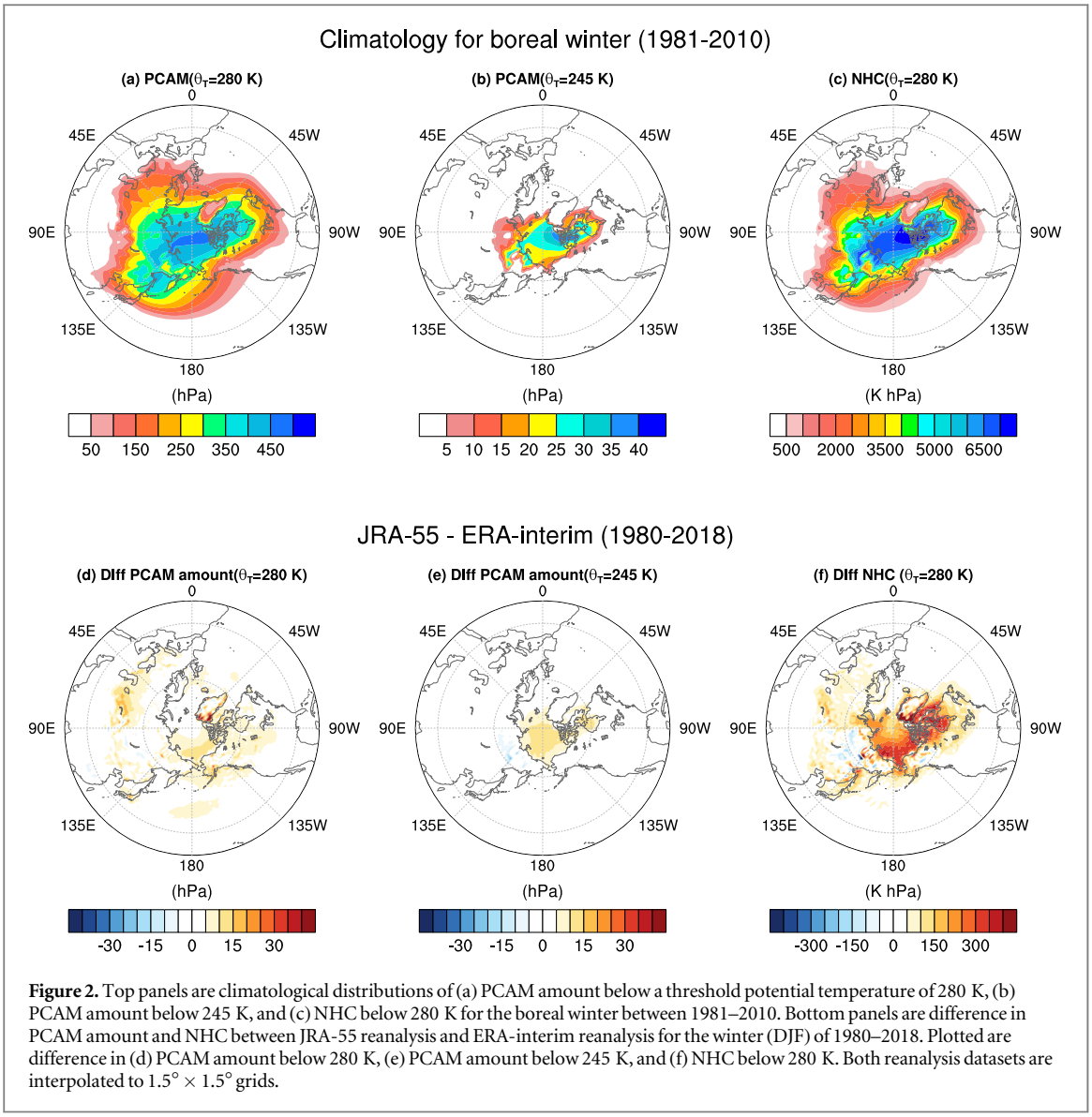

Figure 2. Top panels are climatological distributions of (a) PCAM amount below a threshold potential temperature of 280 K, (b) PCAM amount below 245 K, and (c) NHC below 280 K for the boreal winter between 1981–2010. Bottom panels are difference in PCAM amount and NHC between JRA-55 reanalysis and ERA-interim reanalysis for the winter (DJF) of 1980–2018. Plotted are difference in (d) PCAM amount below 280 K, (e) PCAM amount below 245 K, and (f) NHC below 280 K. Both reanalysis datasets are interpolated to 1.5° × 1.5° grids.

PCAM (245 K). In all three cases, the distributions increase poleward over high latitudes, reaching maxima near the North Pole. PCAM (245 K) is generally confined to areas of Arctic sea ice, with an extension into northern Canada and small amounts over northern Siberia. PCAM (280 K) covers a substantially larger area in an elongated region from eastern Asia across the Pole to eastern North America. The spatial pattern of NHC relative to 280 K (figure 2(c)) is very similar to that of PCAM (280 K). Compared with PCAM (280 K), equatorward extensions of NHC are suppressed over the northeastern Pacific and northern Atlantic Oceans, which reflects relatively warmer temperature distributions near the surface over these regions. When the values in figure 2 are integrated spatially and divided by the gravitational acceleration, the total hemispheric values are 2.22×10^{17} kg for PCAM (280 K), 4.75×10^{15} kg for PCAM (245 K), and 2.42×10^{18} K kg for NHC (280 K) (table 1). The corresponding values for the Arctic polar cap (60° −90°N) are also shown in table 1. Relative to the total hemispheric amounts, the percentages of PCAM (280 K), PCAM (245 K) and NHC (280 K) in the Arctic polar cap are 52%, 92%, and 63%, respectively, indicating that the Arctic is home to a much greater percentage of extremely cold air (PCAM (245 K)) than moderately cold air (PCAM (280 K)) or NHC (280 K).

If PCAM and NHC are to be widely used as indicators, their sensitivities to the data source (i.e. the reanalysis) need to be addressed. Accordingly, we repeated the calculations of the fields in figures 2(a)–(c) with another reanalysis, the European Center for Medium-range Weather Forecasts (ECMWF)-Interim reanalysis, known as ERA-Interim (Dee *et al* 2011). Figure 2 (bottom row) shows the differences between the JRA-based and the ERA-Interim-based fields of PCAM (280 and 245 K) and NHC (280 K). The differences are generally positive, indicating that the PCAM amount tends to be larger in JRA-55 than in ERA-Interim. The differences in PCAM amount below 280 and 245 K range up to about 15 hPa. In the case of PCAM (245 K), these differences represent substantial

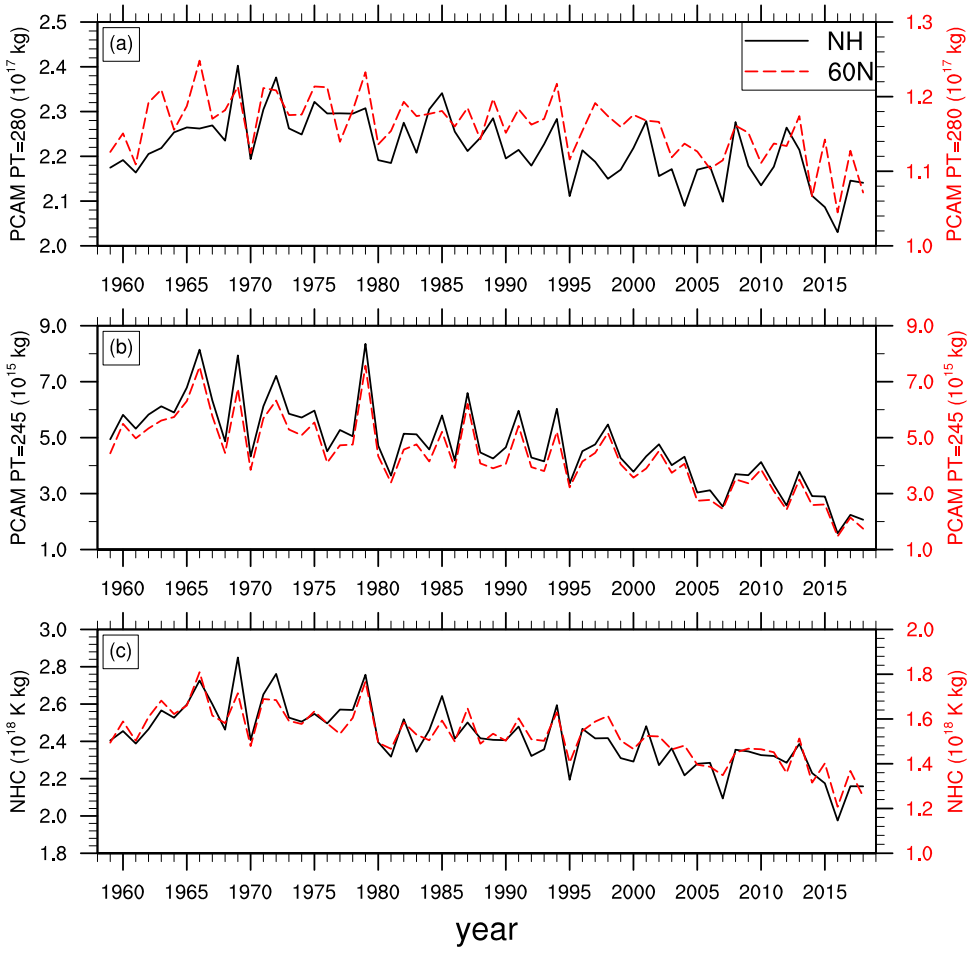

Figure 3. Time series of spatially integrated PCAM amount (a) below 280 K, (b) below 245 K, and (c) NHC below 280 K in the boreal winter. Black solid line (left axis) and red broken line (right axis) denote integration over the Northern Hemisphere and north of 60°N, respectively.

Table 1. Statistics of spatially averaged PCAM amount and NHC. Average values for 60 years (1959–2018), standard deviation of detrended time series, linear trends estimated with the least square method, and *p*-values of the linear trends. The linear trends in the third line are total changes (differences between the final and initial values of linear trend lines) and those in the fourth line are trends divided by averages and the unit is thus %/decade. Suffix –NH (−60N) denotes that PCAM amount or NHC are integrated over the entire Northern Hemisphere (poleward of 60°N).

1959–2018	PCAM280-NH	PCAM245-NH	NHC-NH	PCAM280-60N	PCAM245-60N	NHC-60N
Average	2.22×10^{17}	4.75×10^{15}	2.42×10^{18}	1.16×10^{17}	4.36×10^{15}	1.53×10^{18}
Standard deviation (detrended)	6.20×10^{15}	9.47×10^{14}	1.18×10^{17}	3.41×10^{15}	8.49×10^{14}	8.05×10^{16}
Trend (total change)	-1.34×10^{16}	-3.75×10^{15}	-4.07×10^{17}	-7.17×10^{15}	-3.44×10^{15}	-2.86×10^{17}
Trend (%/decade)	−1.00	−13.2	−2.81	−1.03	−13.2	−3.12
p-value	1.24×10^{-5}	1.60×10^{-12}	2.39×10^{-10}	1.84×10^{-05}	1.21×10^{-12}	9.41×10^{-11}

The units of averages, standard deviation, and trend (total change) for PCAM are kg and for NHC is K kg.

fractions of the total, as the climatological amounts in JRA-55 are typically 20–40 hPa over the Arctic Ocean (figure 2(b)). The fact that the largest differences are found over the sea ice area of the Arctic Ocean suggests that different specifications or treatments of sea ice in the two reanalyses may be contributing to the differences in the cold airmass metrics. The differences in the other integrated measures, PCAM (280 K) and NHC (280 K), are much smaller fractions, generally less than 5%, of the JRA-55 values. Further comparisons among reanalysis datasets are documented in Kanno *et al* (2016).

The time series of the winter-averaged values of PCAM and NHC are shown in figure 3 for the Northern Hemisphere (black lines) for the Arctic (60°−90° N) (red lines). Table 1 summarizes the trends as total changes (differences between final and initial values of linear trend lines) and as percentage changes per

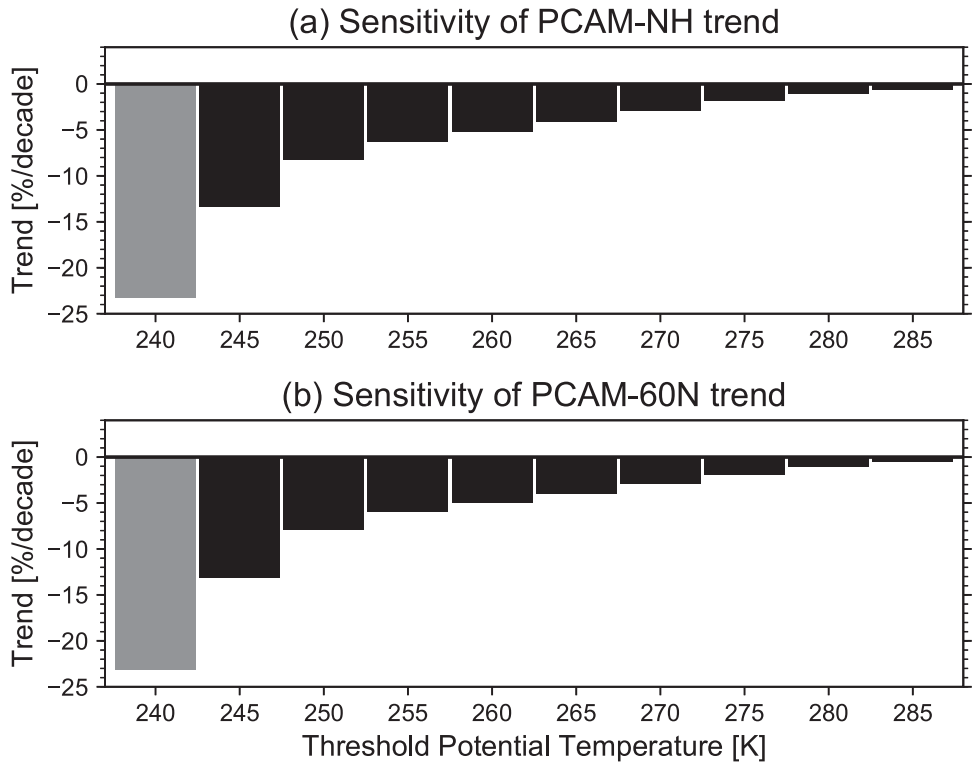

Figure 4. Sensitivity of PCAM trends to the threshold potential temperature. Trends are expressed by slopes of linear trend line divided by average values. Black and gray bars indicate that linear trends satisfy 99% and 95% confidence levels, respectively.

Table 2. Linear trends of NHC below 280 K for different periods. Ratio denotes that the ratio of the NHC trend poleward of 60N to the trend in the Northern Hemisphere and potentially indicates the magnitude of the Arctic amplification.

NHC	Trend (60N) (%/decade)	Trend (NH) (%/decade)	Ratio
1959–2018	−3.16	−2.86	1.11
1959–1988	−1.73	−0.85	2.04
1974–2003	−1.95	−3.02	0.65
1989–2018	−5.62	−3.85	1.46

Trends are normalized by climatological mean values in the reference periods between 1981–2010.

decade. It is apparent that there have been decreases in all the metrics over the 1959–2018 time period, both for the entire Northern Hemisphere and for the Arctic. Interannual variations are superimposed on the decreasing trends, and the interannual variations are larger in magnitude for the hemispheric values than for the Arctic (60°−90°N) values (note the difference in the hemispheric and Arctic scales in figures 3(a) and (c)). The standard deviation of the interannual variations of the detrended PCAM (280 K) and NHC (280 K) are 2%–5% of their climatological mean values, while the standard deviation of the detrended PCAM (245 K) is approximately 20% of its climatological mean. These percentages imply that the amount of extremely cold air is more variable (relative to its mean) on a year-to-year basis than is the amount of moderately cold air.

Despite the interannual variations, the trends are statistically significant at the 99.99% level in all cases. As percent changes per decade, the changes are quite similar for the two domains: approximately −1% per decade for PCAM (280 K), −3% per decade for NHC (280 K), and −13% per decade for PCAM (245 K). The percentage decrease of extremely cold air (PCAM (245 K)) is far greater than the corresponding decreases of moderately cold air, as the loss of PCAM (245 K) over the six decades amounts to about 80%. This large loss is apparent in figure 3(b), which show that the winter-averaged PCAM (245 K) was about 5×10^{15} kg in the 1960s but only about 1×10^{15} kg in the last few years (2016–2018).

Figure 4 provides a more complete documentation of the sensitivity of the trends to the threshold potential temperature. For both the entire Northern Hemisphere (figure 4(a)) and the Arctic (figure 4(b)), the trend of PCAM increases monotonically as the threshold potential temperature is reduced. The trends range from approximately −1% per decade for a threshold of 285 K to approximately −23% per decade for a threshold of 240 K. The sensitivity is greater if the threshold potential temperature is low, whereas it is smaller around the threshold potential temperature of 280 K. For each threshold, the trends are essentially the same for the two domains.

Table 2 is a comparison of the trends in winter-averaged NHC (280 K) during various time periods, including the entire 60 years (1959–2018), the first 30 years (1959–1988), the middle 30 years (1974–2003),

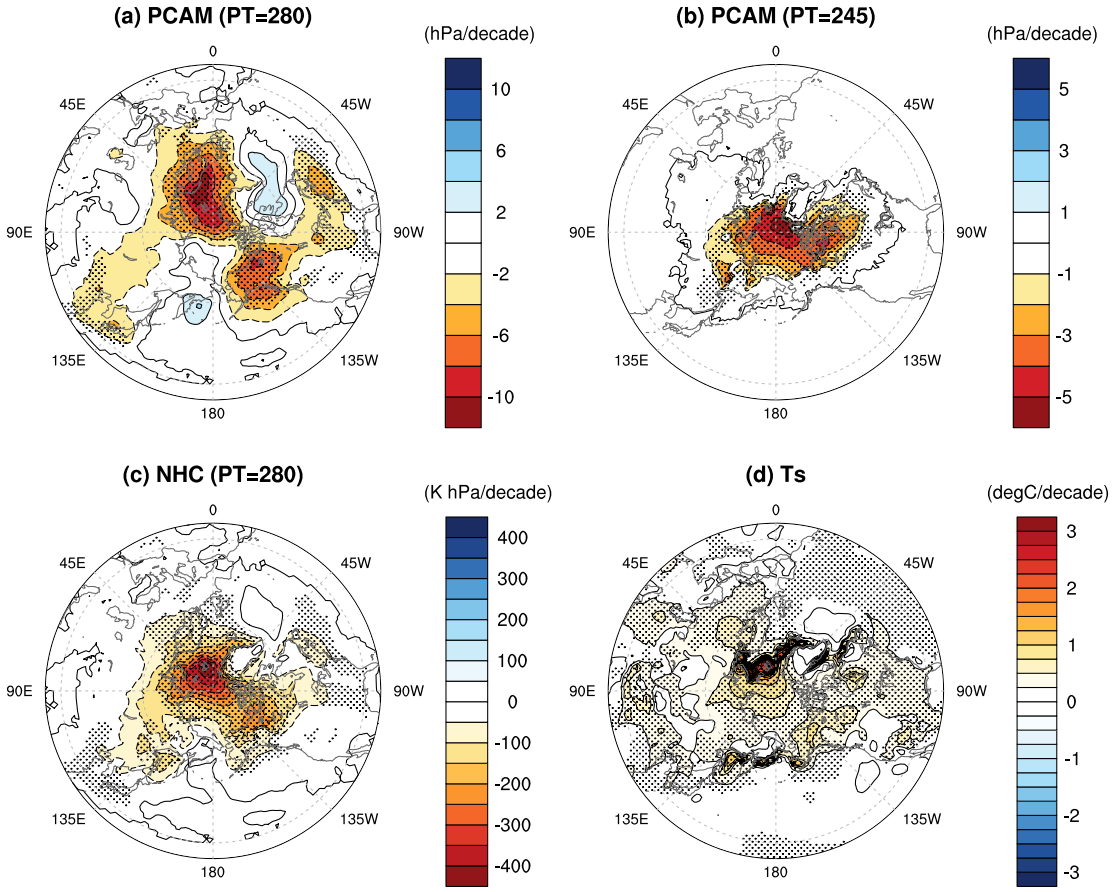

Figure 5. Linear trends of (a) PCAM amount below 280 K, (b) PCAM amount below 245 K, (c) NHC below 280 K, and (d) surface air temperature for the period 1959–2018. Stippling denotes regions in which trends are statistically significant at the 95% confidence level.

and the final 30 years (1989–2018). The trends are shown for both the Arctic polar cap (60°−90°N) and the entire Northern Hemisphere. The largest trends have occurred in the most recent 30 years (1989–2018), for which the trend in the Arctic is approximately 1.8 times larger than the 60 year trend and 3.2 times larger than the mean for the first 30 years. Both the hemispheric and the Arctic trends of NHC show this acceleration over time. Table 2 (right column) also shows that the most recent and the overall trends are greater for the Arctic than for the entire Northern Hemisphere. The spatial patterns of the trends of PCAM and NHC provide another manifestations of Arctic amplification, which has been shown to be a characteristic of Northern Hemisphere temperature variability and trends (e.g. Langen and Alexeev 2007, Pithan and Mauritsen 2014, AMAP 2017).

Figure 5 shows the spatial patterns of the trends of PCAM and NHC, as well as the corresponding trends of surface air temperature over the 60 year period 1959–2018. Both PCAM (280 K) and surface air temperature show spatially complex patterns with maxima over the marginal ice zones of the North Atlantic and the Alaskan region. The various lobes in figure 5(a) for PCAM (280 K) point to an influence of the atmospheric circulation and its modes of internal variability. In the case of surface air temperature (figure 5(d)), the implication is that the recent sea ice loss, amplified by the albedo-temperature feedback, is a key driver of the trends of these variables. The maximum trend of surface air temperature over the seas offshore of Alaska differs from the pattern of PCAM trends (figure 5(a)), which are largest over the land areas of Alaska and the Yukon. This apparent discrepancy appears to be a graphical artifact related to small areas of large warming in the Bering Sea in figure 5(d). Trends of surface air temperature during winter have actually been larger over interior Alaska than over the coastal areas, especially the Bering Sea and Aleutian regions, (http://climate.gi.alaska.edu/ClimTrends/Change/TempChange.html). The trends of PCAM (245 K) and NHC show a more polar-symmetric pattern with the largest trends (decreases) over the Arctic Ocean, especially the Arctic Ocean adjacent to northwestern Canada and Greenland. The patterns of PCAM (245 K) and NHC are indicative of a broader polar amplification, while PCAM (280 K) and surface

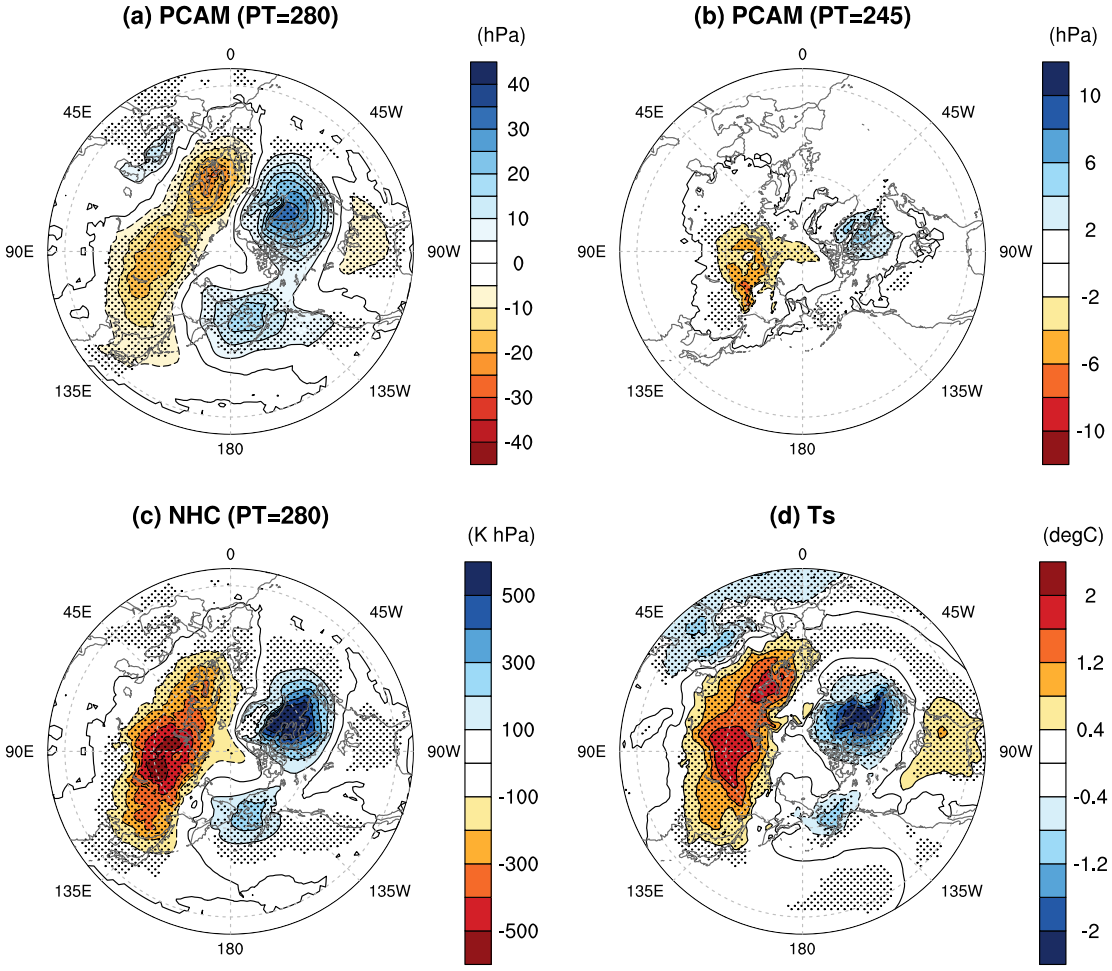

Figure 6. Regressions of (a) PCAM amount below 280 K, (b) PCAM amount below 245 K, (c) NHC below 280 K, and (d) surface air temperature against the AO index. Stippling indicates regions of 95% confidence levels. All regressions were performed on detrended time series.

air temperature appear to be subject to greater influences by modes of internal variability and sea ice loss.

As an illustration of the role of the atmospheric circulation in cold airmass trends, figure 6 shows the results of a regression of various metrics of coldness on the Arctic Oscillation (AO) index. All regressions were performed on detrended time series. The regression patterns of PCAM (280 K) and NHC (280 K) in figures 6(a) and (c) are quite similar to the regression pattern for surface air temperature (figure 6(d)). A seesaw between the western and eastern hemispheres is an outstanding feature of all three patterns, although the NHC pattern shows a single lobe of negative values over Asia rather than the double-lobe pattern shown by PCAM (280 K) and surface air temperature. The regression pattern for PCAM (245 K) in figure 6(b) is considerably weaker, implying that the AO has less influence on interannual variations of extremely cold air than it does on PCAM (280 K) and surface air temperature.

In order to provide a more comprehensive summary of the linkages to modes of variability, table 3 shows the correlations between yearly (detrended) values of the metrics of coldness and indices of the AO, the Niño-3.4 index, the Tropical Northern Hemisphere pattern, the Pacific Decadal Oscillation (PDO) and the Atlantic Multidecadal Oscillation (AMO). All indices were obtained from NOAA Climate Prediction Center, (http://cpc.ncep.noaa.gov/data/indices/). Table 3 shows that the AO is indeed significantly correlated with the hemispheric total NHC (280 K), although not with the corresponding NHC for 60°−90°N. This result is consistent with figure 6(c), in which much of the negative lobe of the regression pattern is south of 60°N. The portion of the Eurasian lobe north of 60°N is largely offset by positive lobes in the North American sector. The same seesaw pattern explains why the correlation between the AO and PCAM (280 K) is not statistically significant, even though the AO correlates almost as strongly with PCAM (245 K) as with NHC (280 K).

PCAM (280 K) for both the Northern Hemisphere and the Arctic show significant correlation with the

Table 3. Correlations between spatially integrated PCAM amount or NHC and teleconnection indices for the period between 1959–2016. Correlation coefficients are calculated after linear trends are removed from all time series.

1959–2016	PCAM280-NH	PCAM245-NH	NHC-NH	PCAM280-60N	PCAM245-60N	NHC-60N
AO	−0.001	−0.245	−0.295*	0.125	−0.239	−0.185
Nino3.4	−0.394*	0.062	−0.200	−0.287*	0.074	−0.095
TNH	0.129	−0.162	0.003	−0.091	−0.177	−0.176
PDO	−0.277*	−0.173	−0.199	−0.325*	−0.165	−0.213
AMO	−0.552*	−0.205	−0.402*	−0.382*	−0.169	−0.254

Asterisk (*) indicates statistical significant correlation at 95% confidence levels.

Table 4. Correlations between spatially integrated PCAM amount or NHC and sea ice area in the Northern Hemisphere for the period 1959–2016. The correlation in the second line is results of detrended time series both PCAM and ice area.

1959–2016	PCAM280-NH	PCAM245-NH	NHC-NH	PCAM280-60N	PCAM245-60N	NHC-60N
Correlation	0.585**	0.744**	0.733**	0.573**	0.733**	0.726**
Correlation (detrended)	0.349**	0.390**	0.434**	0.360**	0.360**	0.406**

Asterisk (**) indicates statistical significant correlation at 99% confidence levels.

Niño3.4, PDO and AMO indices. The tropical connection with hemispheric PCAM amount has been further discussed by Abdillah *et al* (2018). The AMO's correlation with the Northern Hemisphere PCAM (280 K) is especially large, $r = -0.55$. Neither PCAM (245 K) nor NHC (280 K) correlates significantly with these indices. A notable result in table 3 is that PCAM (245 K), the amount of extremely cold air, does not correlate significantly with any of the indices. This lack of correlation implies that diabatic heating (specifically, radiative forcing) may be contributing to the strong decrease in the amount of extremely cold air in the Northern Hemisphere. However, there remains the possibility that other modes of internal variability (e.g. the Arctic Dipole mode; Cai *et al* 2018) not examined here could be contributing to the trends.

Sea ice cover is an additional consideration in the discussion of possible diabatic heating effects. Table 4 shows the correlation between PCAM and arctic sea ice area. Here, sea ice concentration data from HadISST1 are used (Rayner *et al* 2003) to compute the winter ice-covered area. Sea ice area in the Northern Hemisphere shows a strong positive correlation with extremely cold airmasses (PCAM 245) and NHC. Even after the data are detrended, the correlations are significant at the 99% level. The correlations suggest that reduced sea ice may indeed contribute to the decrease in extremely cold air mass. However, such inferences are confounded by the possibility that extremely cold air, in turn, contributes extensive sea ice cover by favoring greater-than-normal freezing of the ocean surface.

4. Conclusion

This study has demonstrated the use of Arctic indicators that depict the amount of cold air mass in the Arctic, including an indicator of the amount of extremely cold air mass. The evaluation of winter trends and variations spans the past 60 years. Because the metrics of coldness contain information from multiple layers in the atmosphere, they provide a more comprehensive framework for assessment of warming than is provided by surface air temperatures alone. Among the key findings obtained here are the following:

- The negative trend of NHC and PCAM based on a colder threshold are stronger (as a % per decade) than the trend of PCAM based on the more moderate threshold, indicating that the loss of extremely cold air is happening at a faster rate than the loss of moderately cold air.
- The most recent time period (1989–2018) shows the most rapid loss of NHC, indicating an acceleration of the loss of cold air.
- The spatial patterns of the trends of PCAM and NHC provide another manifestation of the Arctic amplification.
- Correlations between the metrics of coldness and indices of several major modes of atmosphere-ocean variability show that the amount of extremely cold air does not correlate significantly with the major atmosphere/ocean indices. Of the various teleconnection indices, the AMO shows the strongest correlations with the spatially integrated metrics of moderate coldness (PCAM 280 K and NHC).

The lack of correlation between extremely cold air mass amount (PCAM (245 K)) and modes of internal variability points to other drivers of the trends of extremely cold air mass (figure 3; tables 1 and 2). Modes of variability not considered here are among the possible drivers, and the Arctic Dipole (Cai *et al* 2018) is one such possibility. Radiative forcing

associated with increasing greenhouse gas concentrations is also a candidate explanation, and it is consistent with the finding by Fyfe *et al* (2013) that the recent Arctic warming cannot be explained without a consideration of greenhouse gas forcing. This interpretation is supported by the fact that a signature of greenhouse-gas-driven global warming is a more rapid increase of extreme minimum temperatures than of extreme maximum temperatures (Sillman *et al* 2013, IPCC 2013, USGCRP 2014). However, more robust diagnostic studies are required to determine the relative importance of radiative forcing and dynamical variability of the atmospheric circulation. A challenge in such an assessment is that external forcing can impact modes variability of the atmospheric circulation.

Regardless of the drivers, the results obtained here show that extremely cold air mass in the Arctic has undergone a dramatic reduction (by about 80%) over the past 60 years. The magnitude of this decrease suggests that the cold air mass metrics used here are robust indicators of change that should be part of a continued monitoring for change in the Arctic and the broader climate system.

The loss of extremely cold airmasses also has implications for humans and for ecosystems in the marine and terrestrial domains. For humans, fewer cold extremes will make the Arctic a less formidable environment during the cold season. In addition, cold air outbreaks affecting middle latitudes will be moderated if the current trends continue. The expectation that moderation of cold airmasses will more than offset any increase in frequency and/or duration of cold air outbreaks has already been expressed by Screen *et al* (2015). In a more local context, the absence of cold extremes will reduce risks to wildlife survival (e.g. Klein *et al* 2009), although they may also increase the survivability of pests and other invasive species that adversely affect ecosystems. Alaska's spruce bark beetle outbreak of the past few decades is one such example (Berg *et al* 2006).

Finally, the trends of extremely cold air mass shown here need to be placed into a more comprehensive diagnostic framework. Changes in atmospheric humidity and cloudiness, for example, play important roles in winter temperatures (Kapsch 2016, Cullather *et al* 2016), as does the coverage of snow and sea ice during the winter season. Sea ice is already implicated in the changes of PCAM, as shown by the results in section 3. Changes in sea ice and the other drivers of the surface energy budget have yet to be placed into a quantitative framework to enable an assessment of the relative importance of different variables and processes. Our hope is that the documentation of cold air mass indicators presented here will stimulate broader assessments of the physical and dynamical drivers of cold air mass trends and variations.

Acknowledgments

We would like to express sincere thanks to two anonymous reviewers for their constructive comments. This work was supported in part by the NOAA Climate Program Office through Grant NA17OAR4310160 and by the Japan Society for the Promotion of Science (JSPS) through Grant-in-Aid 15H02129. YK is supported by JSPS through a Grand-in-Aid for Research Fellow (18J01336) and by the FY 2018 Researcher Exchange Program between JSPS and Research Council of Norway.

ORCID iDs

Yuki Kanno https://orcid.org/0000-0001-7587-6697

References

Abdillah M R, Kanno Y and Iwasaki T 2018 Strong linkage of El Niño–Southern Oscillation to the polar cold air mass in the Northern Hemisphere *Geophys. Res. Lett.* **45** 5643–52

AMAP 2017 Snow, Water, Ice and Permafrost in the Arctic: Summary for Policy-Makers Arctic Monitoring and Assessment Programme p 20

Bekryaev R V, Polyakov I V and Alexeev V A 2010 Role of polar amplification in long-term surface air temperature variations and modern arctic warming *J. Clim.* **23** 3888–906

Berg E, Henry J D, Fastie C L, De Volder A D and Matsuoka S M 2006 Spruce beetle outbreaks on the Kenai Peninsula, Alaska, and Kluane National Park and Reserve, Yukon Territoru: relationship to summer temperatures and regional differences in disturbance regimes *Forest Ecol. Manage.* **3** 219–32

Cai L, Alexeev V A, Walsh J E and Bhatt U S 2018 Patterns, impacts, and future projections of summer variability in the Arctic from CMIP5 models *J. Clim.* **31** 9815–33

Cullather R L, Lim Y-K, Boisvert L N, Brucker L, Lee J N and Nowicki S M J 2016 Analysis of the warmest Arctic winter, 2015–2016 *Geophys. Res. Lett.* **43** 808–10

Dee D *et al* 2011 The ERA-Interim reanalysis: configuration and performance of the data assimilation system *Quart. J. Roy. Meteor. Soc* **137** 553–97

Fyfe J C, von Salzen K, Gillett N P, Arora V K, Flato G and McConnell J R 2013 One hundred years of Arctic surface temperature variation due to anthropogenic influence *Nat. Sci. Rep.* **3** 2645

Graham R M, Cohen L, Petty A A, Boisvert L N, Rinke A, Hudson S R, Nicolaus M and Granskog M A 2017 Increasing frequency and duration of Arctic winter warming events *Geophys. Res. Lett.* **44** 6974–83

IPCC *et al* 2013 *Climate Change 2013: The Physical Science Basis. Contribution of Working Group I to the Fifth Assessment Report of the Intergovernmental Panel on Climate Change* ed T F Stocker *et al* (Cambridge: Cambridge University Press)

Iwasaki T and Mochizuki Y 2012 Mass-weighted isentropic zonal mean equatorward flow in the Northern Hemispheric winter *Sci. Online Lett. Atmos.* **8** 115–8

Iwasaki T, Shoji T, Kanno Y, Sawada M, Ujiie M and Takaya K 2014 Isentropic analysis of polar cold airmass streams in the Northern Hemispheric winter *J. Atmos. Sci.* **71** 2230–43

Kanno Y, Shoji T and Iwasaki T 2015 Comparison study of the polar cold air mass between Northern and Southern Hemispheric winters based on a zonal-mean two-box model *Atmos. Sci. Lett* **16** 70–6

Kanno Y, Abdillah M R and Iwasaki T 2016 Long-term trend of cold air mass amount below a designated potential temperature in

Northern and Southern Hemispheric winters using reanalysis data sets *J. Geophys. Res.-Atmos* **121** 10138–52
Kanno Y, Walsh J E and Iwasaki T 2017 Interannual variability of the North American cold air stream and associated synoptic circulations *J. Clim.* **30** 9575–90
Kapsch M-L 2016 The effect of downwelling longwave and shortwave radiation on Arctic summer sea ice *J. Clim.* **29** 1143–59
Kaufman D S, Schneider D P, McKay N P, Ammann C M, Bradley R S, Briffa K R, Miller G H, Otto-Bliesner B L, Overpeck J T, Vinther B M and Arctic Lakes 2 K Project Members 2009 Recent warming reverses long-term Arctic cooling *Science* **325** 1236
Klein D, Walsh J E and Shulski M 2009 What killed the reindeer of St. Matthew Island? *Weatherwise* **62** 32–9
Kobayashi S *et al* 2015 The JRA-55 reanalysis: general specifications and basic characteristics *J. Meteor. Soc. Japan* **93** 5–48
Langen P L and Alexeev V A 2007 Polar amplification as a preferred response in an idealized qaquaplanet GCM *Clim. Dyn.* **29** 305–17
Mori M, Watanabe M, Shiogama H, Inoue J and Kimoto M 2014 Robust Arctic sea-ice influence on the frequent Eurasian cold winters in past decades *Nat. Geosci.* **7** 869–73
Overland J E, Hanna E, Hanssen-Bauer I, Kim S -J, Walsh J E, Wang M, Bhatt U S and Thoman R L 2017 Arctic Report Card *Surface air temperature* National Oceanic Atmospheric Administration (https://arctic.noaa.gov/Report-Card/Report-Card-2018/ArtMID/7878/ArticleID/783/Surface-Air-Temperature)
Ogawa F *et al* 2018 Evaluating impacts of recent Arctic sea ice loss on the northern hemisphere winter climate change *Geophys. Res. Lett.* **45** 3255–63
Overland J E and Wang M 2018 Arctic-midlatitude weather linkages in North America *Polar Sci.* **16** 1–9
Pithan F and Mauritsen T 2014 Arctic amplification dominated by temperature feedbacks in contemporary climate models *Nat. Geosci.* **7** 181–4
Rayner N A, Parker D E, Horton E B, Folland C F, Alexander L V, Rowell D P, Kent E C and Kaplan A 2003 Global analyses of sea surface temperature, sea ice, and night marine air temperature since the late nineteenth century *J. Geophys. Res.* **108** 4407
Screen J A, Deser C and Sun L 2015 Reduced risk of North American cold extremes due to continued Arctic sea ice loss *Bull. Am. Meteor. Soc.* **96** 1489–503
Serreze M C, Barrett A P and Stroeve J 2012 Recent changes in tropospheric water vapor over the Arctic as assessed from radiosondes and atmospheric reanalyses *J. Geophys. Res.* **117** D10104
Sillmann J, Kharin V V, Zhang X, Zwiers F W and Bronaugh D 2013 Climate extremes indices in the CMIP5 multimodel ensemble: I. Model evaluation in the present climate *J. Geophys. Res. (Atmos.)* **118** 1716–33
USGCRP 2014 *Highlights of Climate Change Impacts in the United States* ed J M Melillo, T C Richmond and G Yohe (Washington, DC: U.S. Global Change Research Program) pp 137